Evaluation of hydrometeor types and properties in the ICON-LAM model with polarimetric radar observations

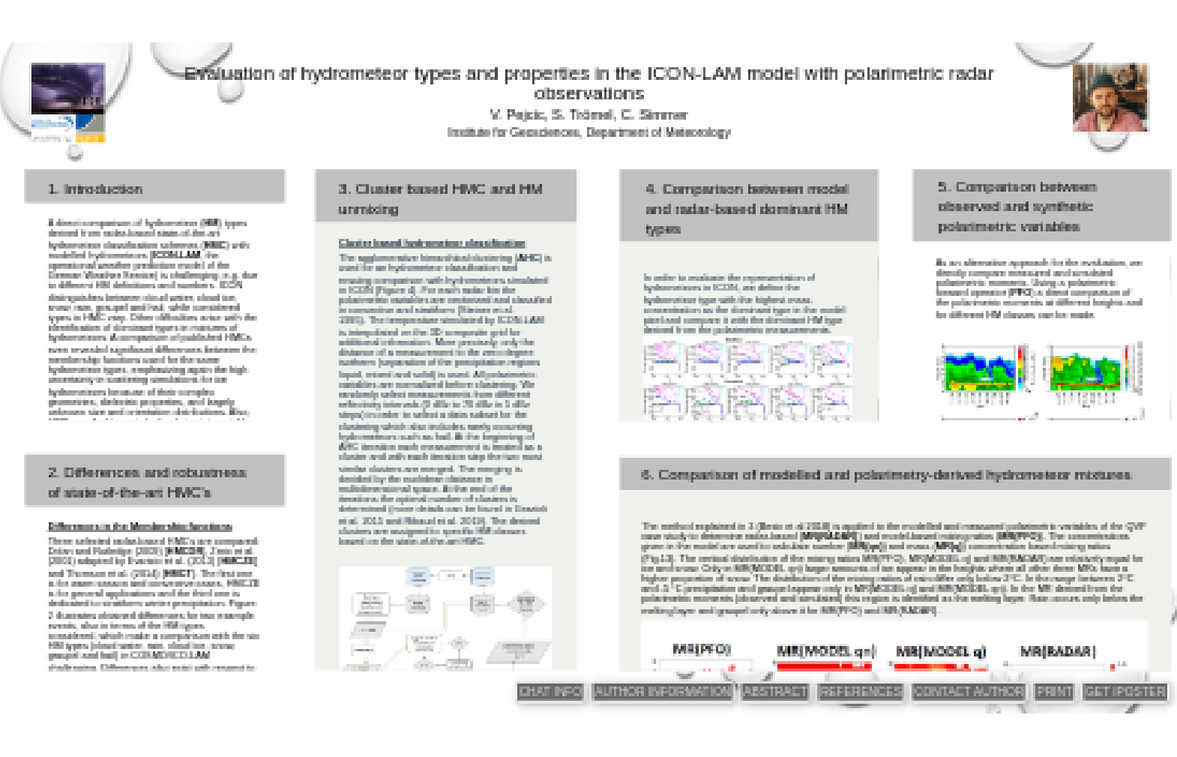

V. Pejcic, S. Trömel, C. Simmer

Institute for Geosciences, Department of Meteorology

PRESENTED AT:

AGU FALL MEETING

Online Everywhere | 1–17 December 2020

1. INTRODUCTION

A direct comparison of hydrometeor (**HM**) types derived from radar-based state-of-the-art hydrometeor classification schemes (**HMC**) with modelled hydrometeors (**ICON-LAM**, the operational weather prediction model of the German Weather Service) is challenging, e.g. due to different HM definitions and numbers. ICON distinguishes between cloud water, cloud ice, snow, rain, graupel and hail, while considered types in HMC vary. Other difficulties arise with the identification of dominant types in mixtures of hydrometeors. A comparison of published HMCs even revealed significant differences between the membership functions used for the same hydrometeor types, emphasizing again the high uncertainty in scattering simulations for ice hydrometeors because of their complex geometries, dielectric properties, and largely unknown size and orientation distributions. Also, HMCs applied to perturbed polarimetric variables observed by the X-band Radar in Bonn (**BoXPol**), Germany, reveal misclassifications especially in the regions with solid precipitation. Thus, a dual strategy to evaluate the representation of hydrometeor type in ICON-LAM is motivated:

i) Classification after clustering of the radar data is assumed to reduce the sensitivity of HMCs to the uncertainty of scattering simulations. An agglomerative hierarchical clustering of the radar pixels based on their similarity in multi-dimensional polarimetric signatures is performed and for each identified cluster the distributions of polarimetric moments are compared to scattering simulations or membership functions for different HM types. Additionally, the centroids of the clusters are used to estimate the mixing ratios of the different HM (Besic et al. 2018).

ii) A direct comparison of multivariate forward-simulated and observed distributions of polarimetric moments serves as a second approach for evaluation. These comparisons are performed for different heights and/or space-time subsets, and for clusters with similar HM in the model and the observations as identified with the advanced radar-based hydrometeor classification scheme (see first strategy).

Results for a set of ten case study days observed with the polarimetric X-band radar composite (Figure 1.) located in western Germany, are presented.

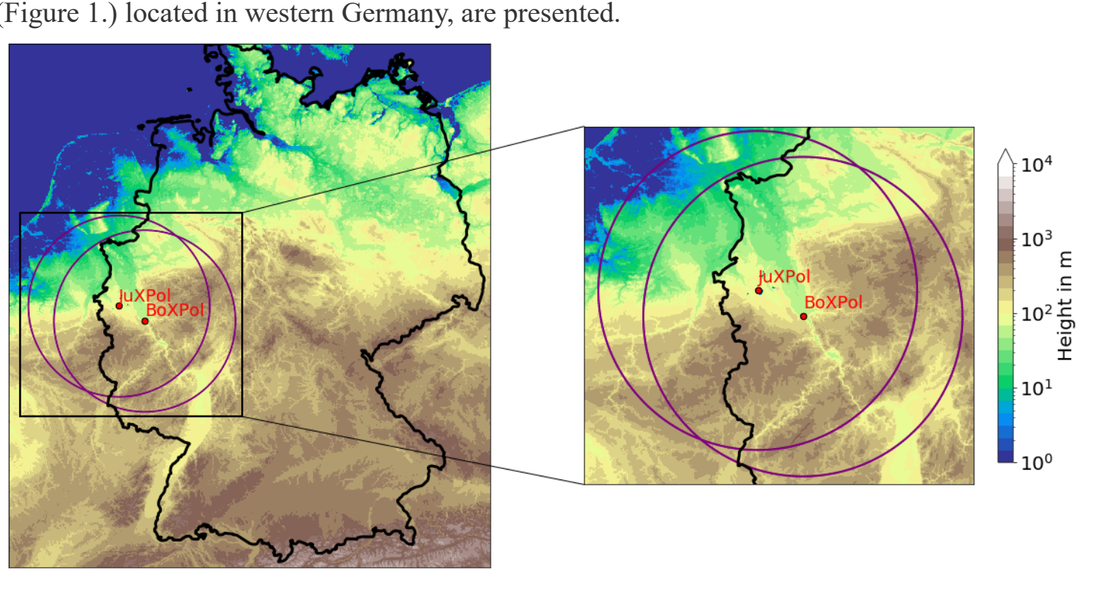

Figure 1.: Location of the polarimetric X-band radar composite consisting of two twin X-Band radars located in Bonn (BoXPol) and Jülich (JuXPol), Germany.

2. DIFFERENCES AND ROBUSTNESS OF STATE-OF-THE-ART HMC'S

Differences in the Membership functions

Three selected radar-based HMC's are compared: Dolan and Rutledge (2009) [**HMCDR**], Zrnic et al. (2001) adapted by Evaristo et al. (2013) [**HMCZE**] and Thomson et al. (2014) [**HMCT**]. The first one is for warm season and convective cases, HMCZE is for general applications and the third one is dedicated to stratiform winter precipitation. Figure 2 illustrates obtained differences for two example events, also in terms of the HM types considered, which make a comparison with the six HM types (cloud water, rain, cloud ice, snow, graupel and hail) in COSMO/ICO-LAM challenging. Differences also exist with respect to the methodology. HMCZW uses bivariate membership functions, while the others use univariate membership function. HMCT first separates liquid, solid and mixed precipitation followed by classification within these regimes.

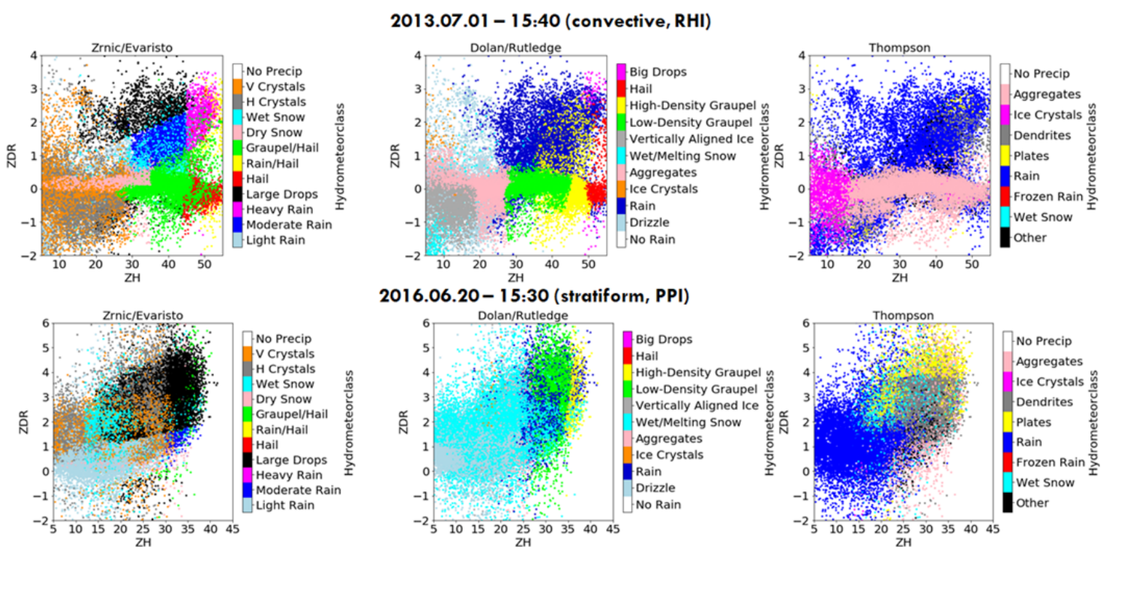

Figure 2. : Two-dimensional projection of horizontal reflectivity against differential reflectivity for the comparison of three HMCs (left column: HMCZE, middle column: HMCDR, right column: HMCT) applied to a range-height-indicator (RHI) scan measured on 1 July 2013 at 15:40 UTC (convective event, top row) and a plan position indicator (PPI) scan measured on 20 February 2016 at 15:30 UTC (stratiform, bottom row) with the X-band radar in Bonn (BoXPol), Germany. The colors indicate the specific HM types of the three different schemes.

Impact of radar observation accuracy on HM typing

In order to assess the impact of uncertainties in radar measurements on HM typing, four example events have been selected and according measurements have been perturbed with the statistical errors expected (Ryzhkov and Zrnic 2019). Assuming the statistical errors of the variables follow a Gaussian distribution, 100 realizations of each of the four events are generated and fed into the HMCs. Resulting normalized distributions of the HM types are illustrated in Figure. 3. Basically, measurement inaccuracies can result in misclassification of any HM type.

Measurements classified by HMCDR and HMCZE with *No Rain* are very often misclassified as *Drizzle/Light Rain*. *Light Rain* is mostly misclassified with HMCDR as *Aggregates* and *Wet Snow* followed by *Rain* and *Low-Density Graupel*. Whereas in HMCZE *Light Rain* can also be misinterpreted as *Vertically/Horizontally Aligned Crystals*. With HMCZE measurement errors lead to pronounced misclassifications within the ice phase.

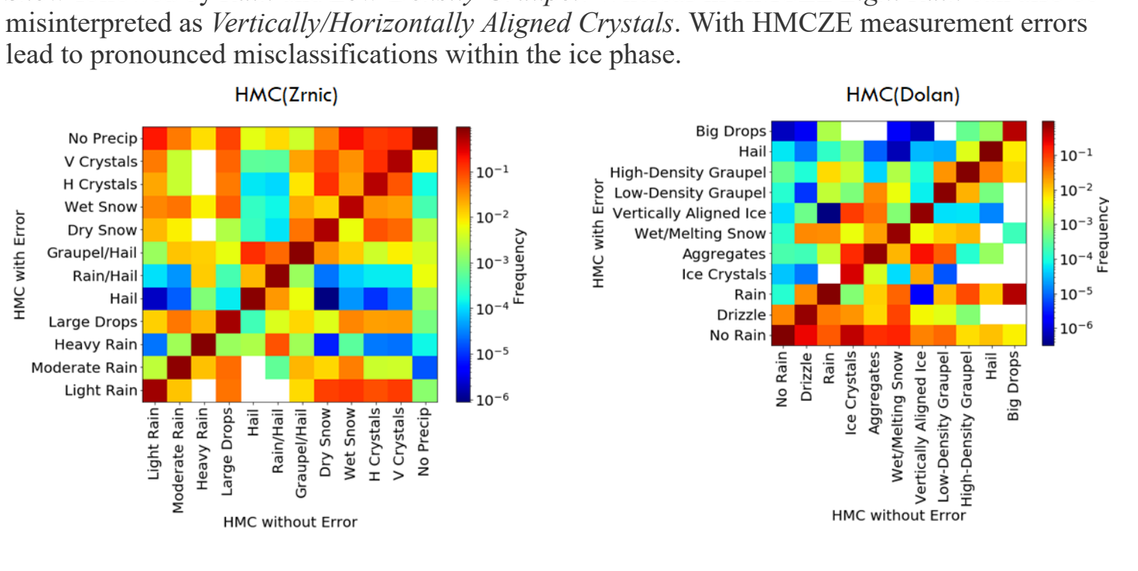

Figure 3.: Hydrometeor typing with perturbed polarimetric variables versus the typing achieved without error perturbation for 100 realisations of four example events (25 June 2016 at 04:10 UTC, 20 June 2016 at 15:30 UTC, 1 July 2013 at 15:40 and at 15:50 UTC. Results are shown for HMCZE (left) and HMCDR (right).

3. CLUSTER BASED HMC AND HM UNMIXING

Cluster based hydrometeor classification

The agglomerative hierarchical clustering (**AHC**) is used for an hydrometeor classification and ensuing comparison with hydrometeors simulated in ICON (Figure 4). For each radar bin the polarimetric variables are vectorized and classified in convective and stratiform (Steiner et al. 1995). The temperature simulated by ICON-LAM is interpolated on the 3D composite grid for additional information. More precisely, only the distance of a measurement to the zero degree isotherm (separation of the precipitation regions liquid, mixed and solid) is used. All polarimetric variables are normalized before clustering. We randomly select measurements from different reflectivity intervals (0 dBz to 70 dBz in 5 dBz steps) in order to select a data subset for the clustering which also includes rarely occurring hydrometeors such as hail. At the beginning of AHC iteration each measurement is treated as a cluster and with each iteration step the two most similar clusters are merged. The merging is decided by the euclidean distance in multidimensional space. At the end of the iterations the optimal number of clusters is determined (more details can be found in Grazioli et al. 2015 and Ribaud et al. 2019). The derived clusters are assigned to specific HM classes based on the state-of-the-art HMC.

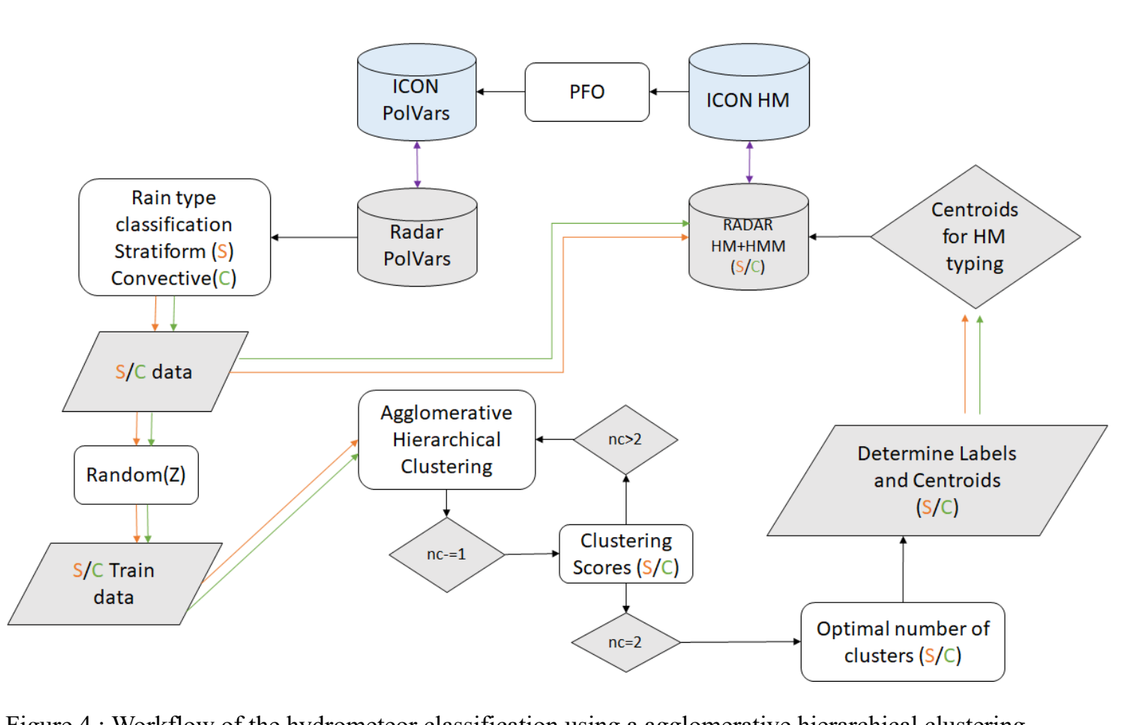

Figure 4.: Workflow of the hydrometeor classification using a agglomerative hierarchical clustering approach

Five clusters are identified for stratiform precipitation (rain (*RN*), snow (*SN*), ice (*CI*), graupel (*GR*) and melting particles (*ML*)) and six for convective precipitation (rain (*RN*), snow (*SN*), ice (*CI*), graupel (*GR*), hail (*HA*) and melting particles (*ML*)). From these resulting clusters (Figure 5) centroids are calculated for each HM type. These are five-dimensional averages of the polarimetric variables of each cluster and are used to assign (depending on the euclidian distance) further measurements to the existing clusters and thus to a specific HM class.

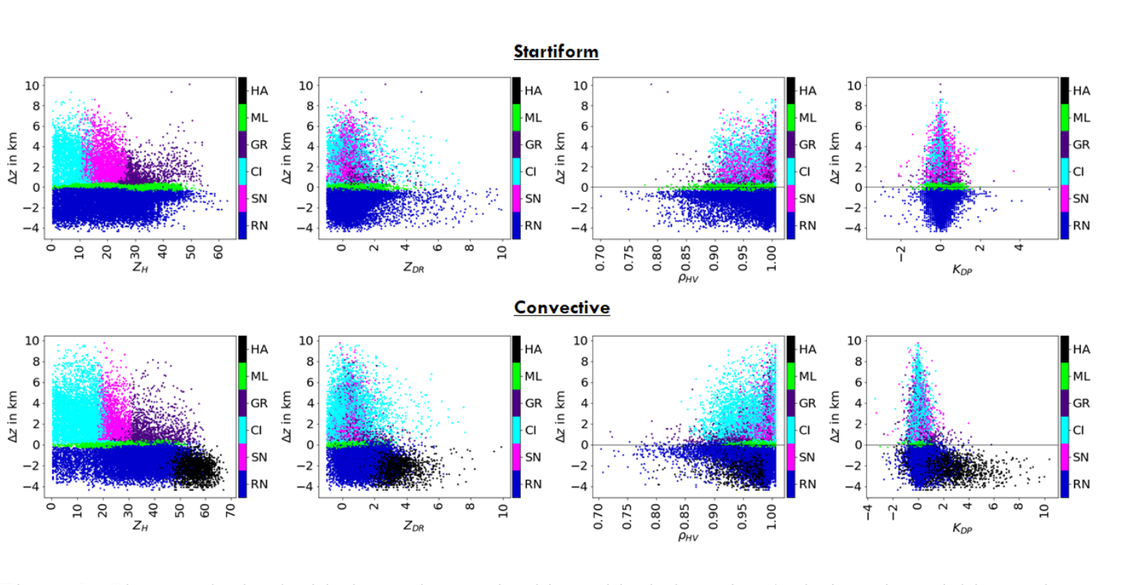

Figure 5.: Clusters obtained with the agglomerative hierarchical clustering (polarimetric variables against relative height to the 0°C isotherm) for stratiform and convective precipitation types. The abbreviations stand for: rain (RN), snow (SN), ice (CI), graupel (GR), hail (HA) and melting particles (ML).

Unraveling of hydrometeor mixtures

Besic at al. (2018) used the distance (d_i) between centroids and measurements to calculate the probability of occurrence of different HM (HM mixing ratios, pi):

$$p_i = e^{-t_i d_i}$$

The index i represents the HM class and the probability depends on the slope (t_i) that can be determined for each HM class considering the distribution of the centroids in the multidimensional space. The entropy is defined as

$$H = -\sum_{i=1}^{n} p_i \log_n p_i$$

and is a measure for the pureness of an observation. A high entropy indicates a mixture of HM in an observation and a low entropy indicates a pure measurement. The probability functions p_i of the individual HM need to be adapted to the surrounding centroids by using the entropy to determine the slope t_i. A synthetic data set is required for this purpose. Here the derived centroids, contaminated with an error of 1%, are defined as pure measurements and a linear combination of two of these pure measurements is defined as a 50%-50% mixture. The entropy of the former should be very low and of the latter high, which is verified with the synthetic data set. The assumptions for a convective precipitation data set are shown in Figure 6. By parameterizing the entropy, the individual slopes of the probability functions can be adjusted. The parametrized entropy shows very low values for synthetic data of pure HM and higher values for the synthetic HM mixtures.

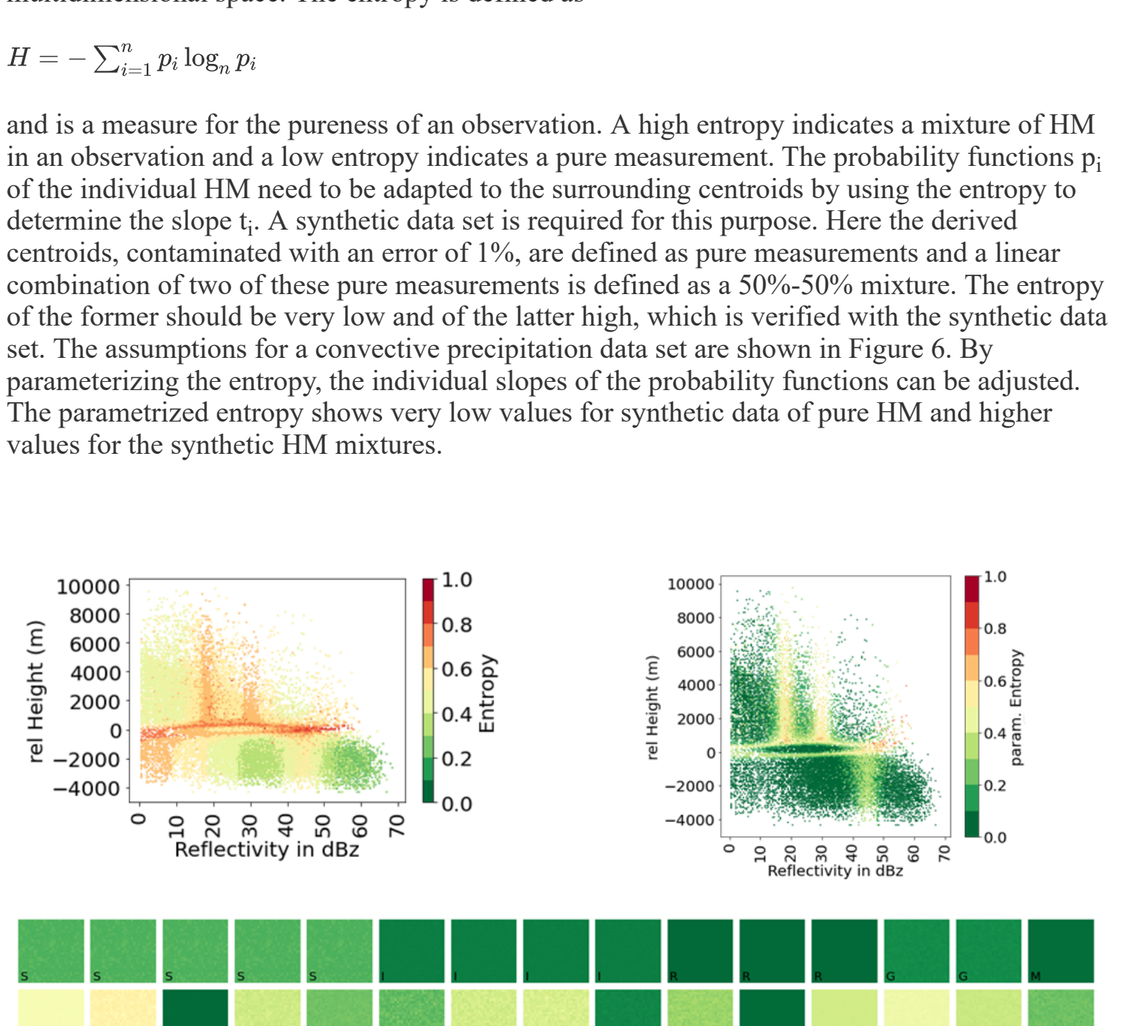

Fig 6.:Non-parametrized (top left) and parametrized entropy (top right) resulting from the entropy of the synthetic data set (bottom). The upper row and the lower row indicate the pure HM classes (900 per box) mixed in 50%-50% proportions (middle row). HM classes considered are rain (R), snow (S), ice (I), graupel (G), melting particles (M) and hail (H).

4. COMPARISON BETWEEN MODEL AND RADAR-BASED DOMINANT HM TYPES

In order to evaluate the representation of hydrometeors in ICON, we define the hydrometeor type with the highest mass concentration as the dominant type in the model pixel and compare it with the dominant HM type derived from the polarimetric measurements.

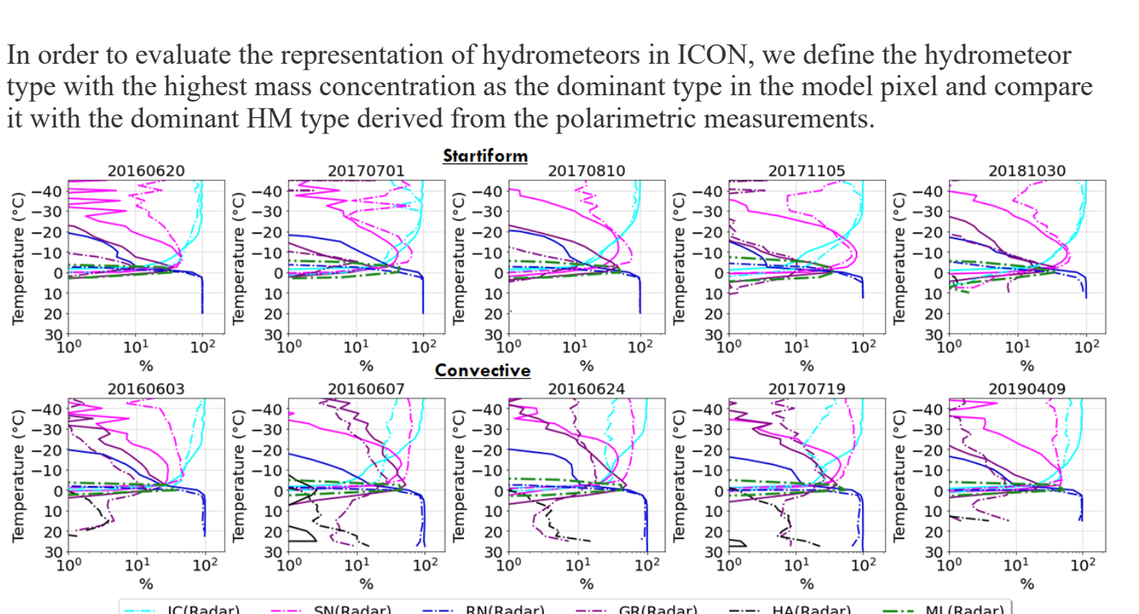

Figure 7.: Comparison between dominant model and radar based hydrometeor types of five convective (bottom) and five stratiform (top) case study days. The dashed lines representing the radar based and the solid lines the model based relative numbers of HM types per 3°C temperature layer..

We found that in stratiform events the model underestimates the proportions of snow hydrometeors and overestimates graupel occurences; the ice proportions show very slight deviations. In convective events the snow underestimation and graupel overestimation are even more pronounced. Below the freezing level modelled graupel and hail occurances are underestimated.

5. COMPARISON BETWEEN OBSERVED AND SYNTHETIC POLARIMETRIC VARIABLES

As an alternative approach for the evaluation, we directly compare measured and simulated polarimetric moments. Using a polarimetric forward operator (**PFO**) a direct comparison of the polarimetric moments at different heights and for different HM classes can be made.

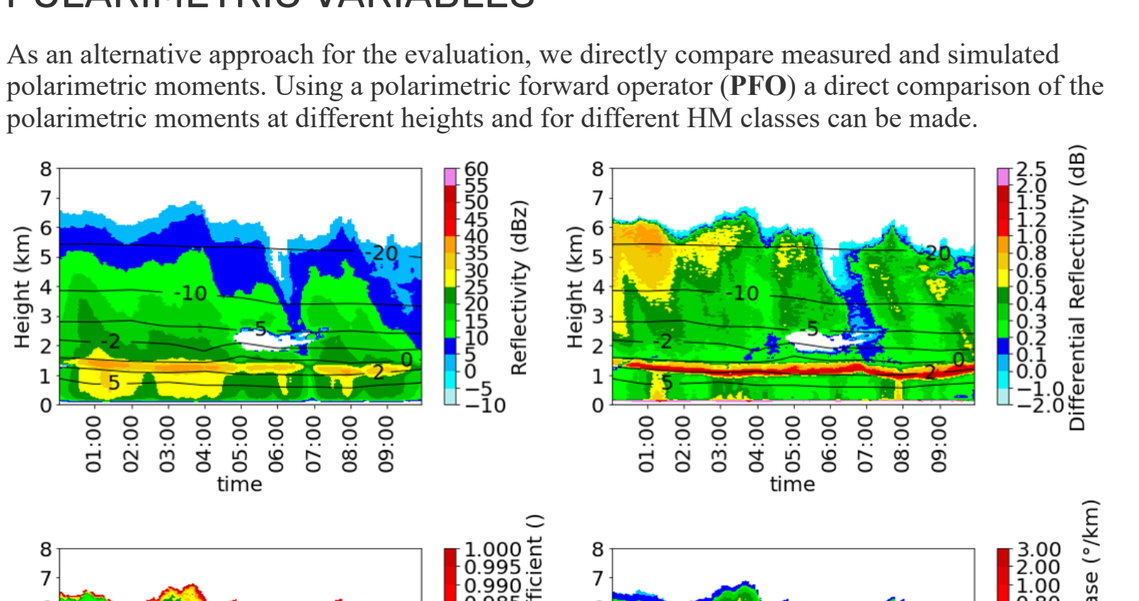

Figure 8.: Quasi-vertical profile (QVP) of a 18° PPI scan measured with BoXPol on 16 November2014 between 00:00 UTC and 10:00 UTC.

A quasi-vertical profile (**QVP,** *azimuthal averege*) based on the 18° PPI scan measured with the BoXPol radar (Figure. 8) is compared to the synthetic variables derived from Cosmo model output in a similar time-space domain (Figure 9.).

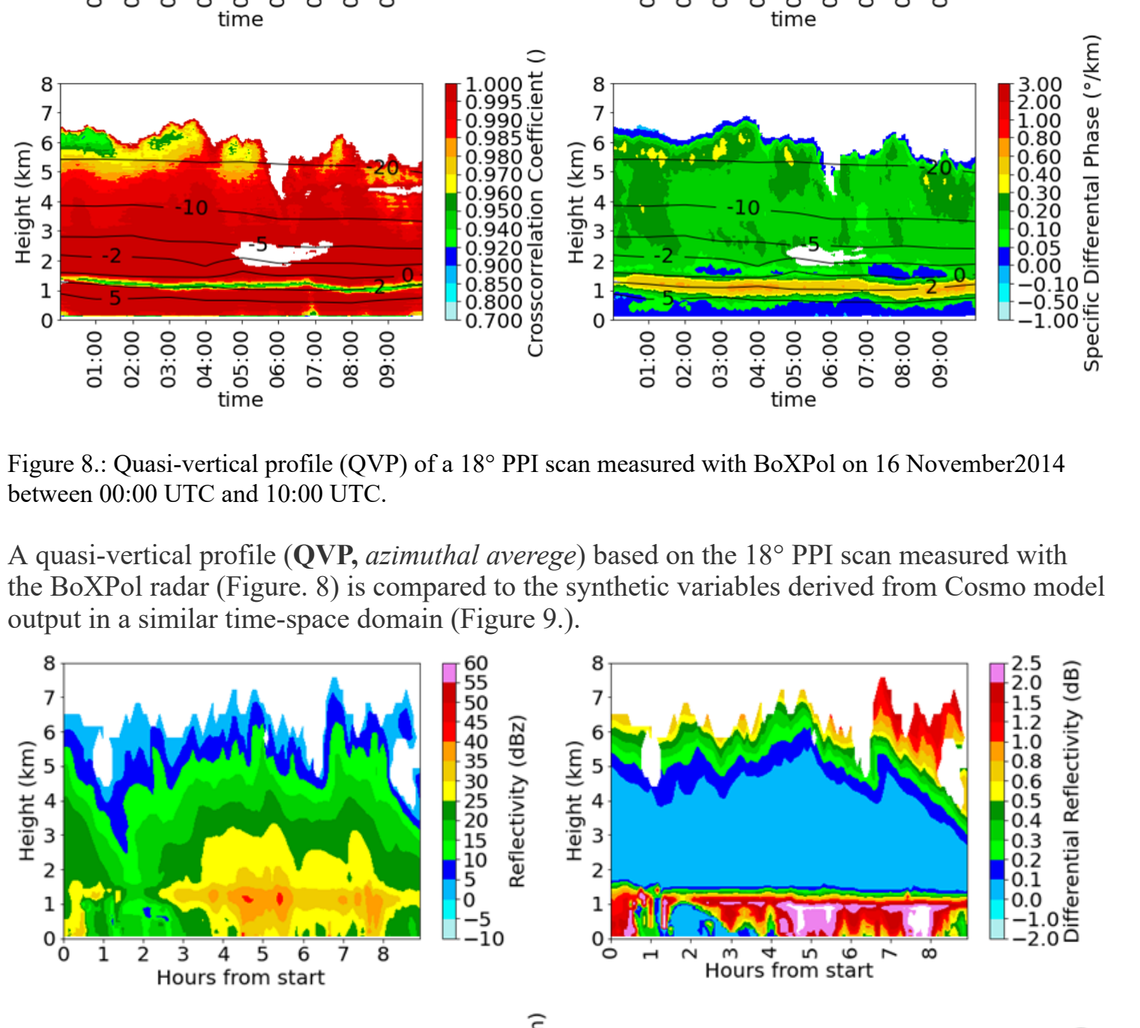

Figure 9.:Synthetic variables dervied from Cosmo model output in a similar time-height display QVPs showing the BoXPol measurements on 16 November 2014 between 00:00 UTC and 10:00 UTC (Fig. 8).

Comparing the profiles of synthetic and observed polarimetric variables (Figure. 10) it can be seen that there is an overestimation of the simulated reflectivity over the freezing level and also an overestimation of the simulated differential reflectivity below the freezing level. The simulated differential reflectivity and specific differential phase above the melting layer are underestimated. The simulated cross correlation coefficient in the melting layer is also underestimated.

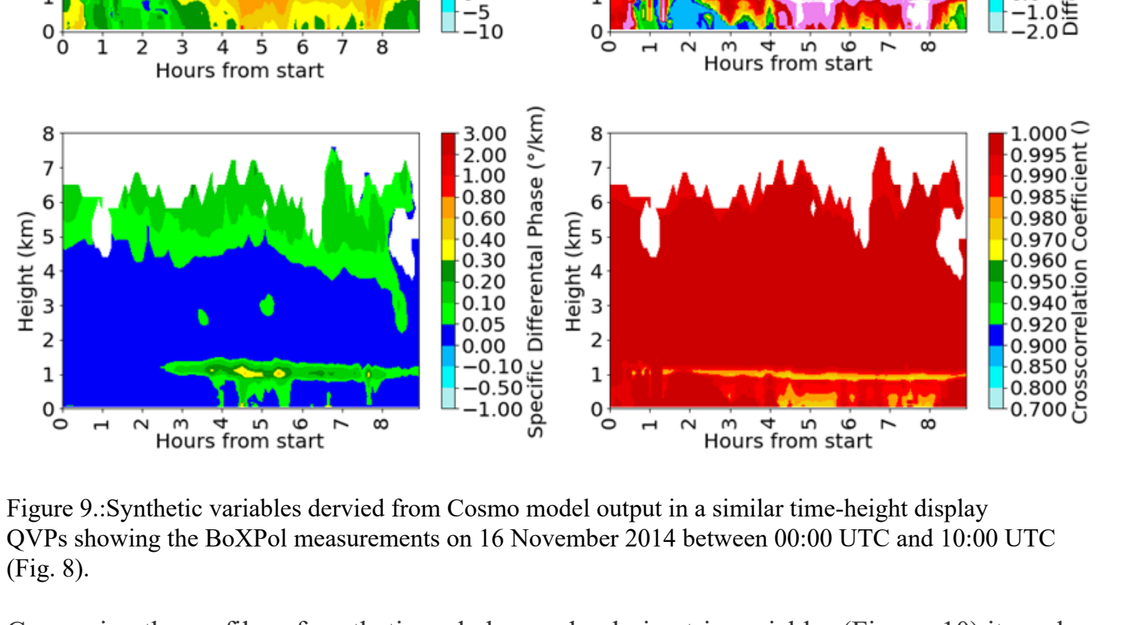

Figure 10.: Comparison between observed (top) and modelled (bottom) polarimetric moments. The horizontal red lines indicate the zero degree height and the vertical black lines the 20 dBz, 0 dB and the 0 °/km values for better visual comparison. The color indicates the number of samples and the boxplots show the quantiles and mean values (blue line in boxplots).

If the simulated and measured polarimetric moments are classified with the different HMCs (Figure 11. and Figure 12.), the overestimation of the reflectivity underestimation of the differential reflectivity often leads to an increased classification of graupel.

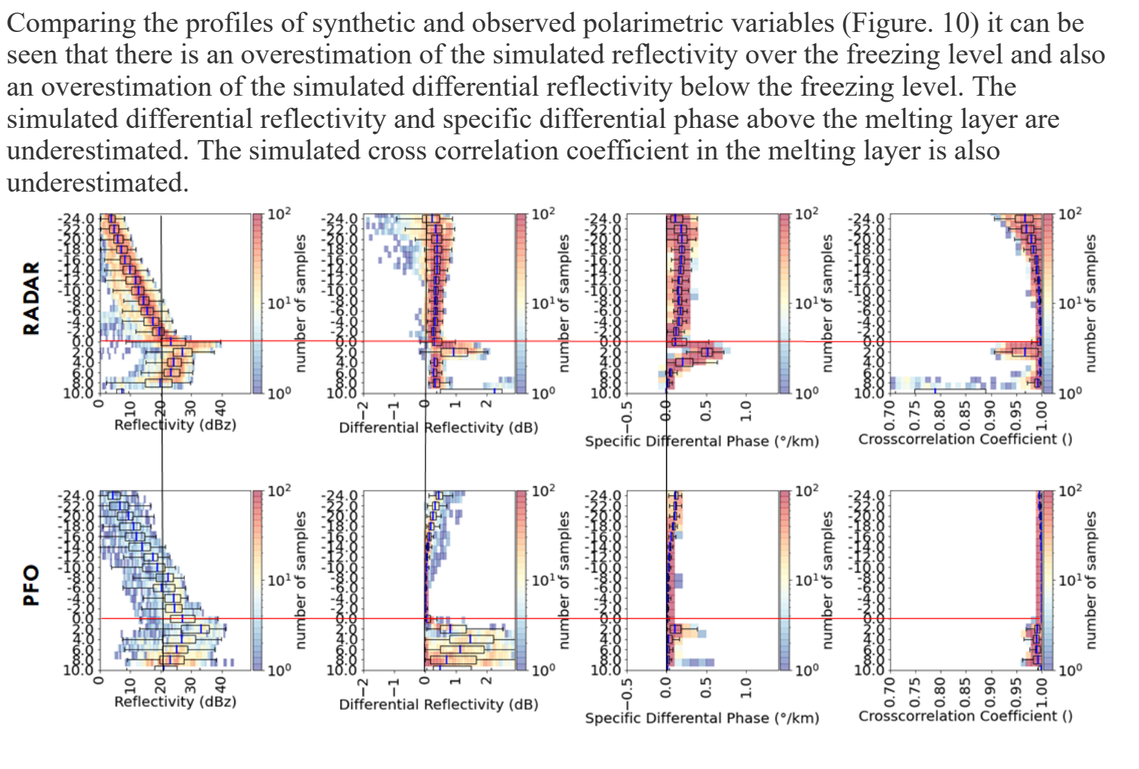

Figure 11.: Hydrometeor classification based on the QVP of a 18° PPI scan measured with BoXPol on 16 November 2014 between 00:00 UTC and 10:00 UTC. Different panels show the cluster-based HMC (top left), HMCT (top right), HMCD (bottom left) and HMCZ (bottom right).

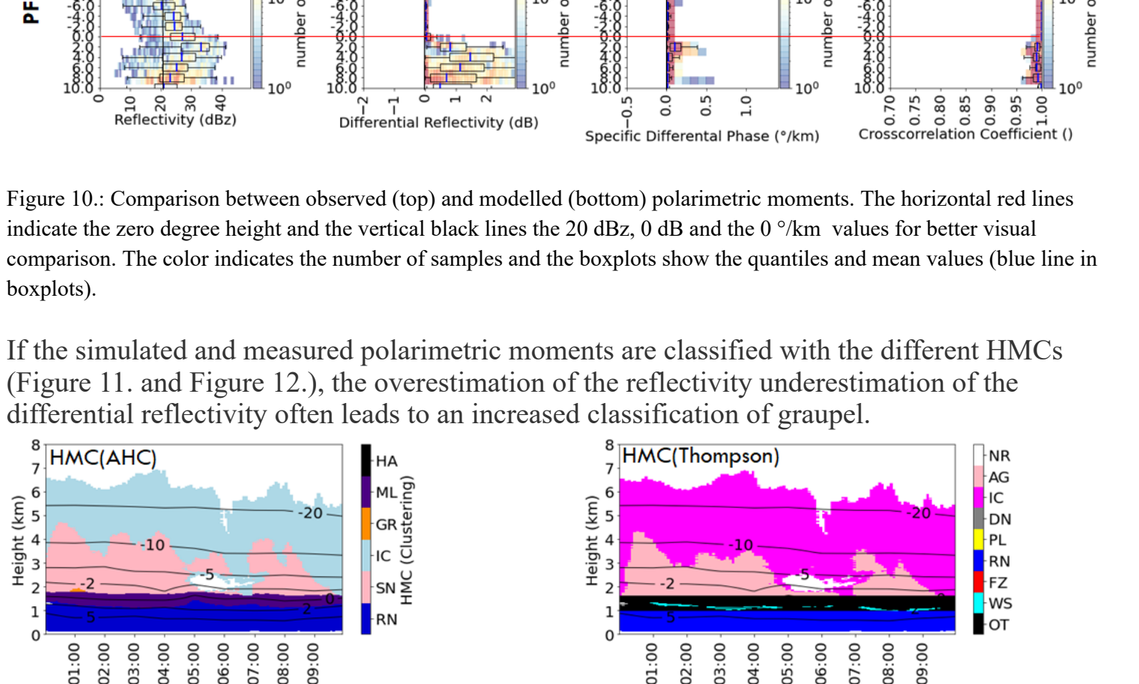

Figure 12.: Hydrometeor classification based on synthetic variables derived from COSMO simulations for 16 November 2014 between 0:00 and 10:00 UTC using a similar time-height display like the QVP shown in Figure. 11. Different panels show the cluster-based HMC (top left), HMCT (top right), HMCD (bottom left) and HMCZ (bottom right).

6. COMPARISON OF MODELLED AND POLARIMETRY-DERIVED HYDROMETEOR MIXTURES

The method explained in 3 (Besic et al 2018) is applied to the modelled and measured polarimetric variables of the QVP case study to determine radar-based (**MR(RADAR)**) and model-based mixing ratios (**MR(PFO)**). The concentrations given in the model are used to calculate number (**MR(qn)**) and mass (**MR(q)**) concentration based mixing ratios (Fig.13). The vertical distribution of the mixing ratios MR(PFO), MR(MODEL q) and MR(RADAR) are relatively equal for ice and snow. Only in MR(MODEL qn) larger amounts of ice appear in the heights where all other three MRs have a higher proportion of snow. The distribution of the mixing ratios of rain differ only below 2°C. In the range between 2°C and -5 °C precipitation and graupel appear only in MR(MODEL q) and MR(MODEL qn). In the MR derived from the polarimetric moments (observed and simulated) this region is identified as the melting layer. Rain occurs only below the melting layer and graupel only above it for MR(PFO) and MR(RADAR).

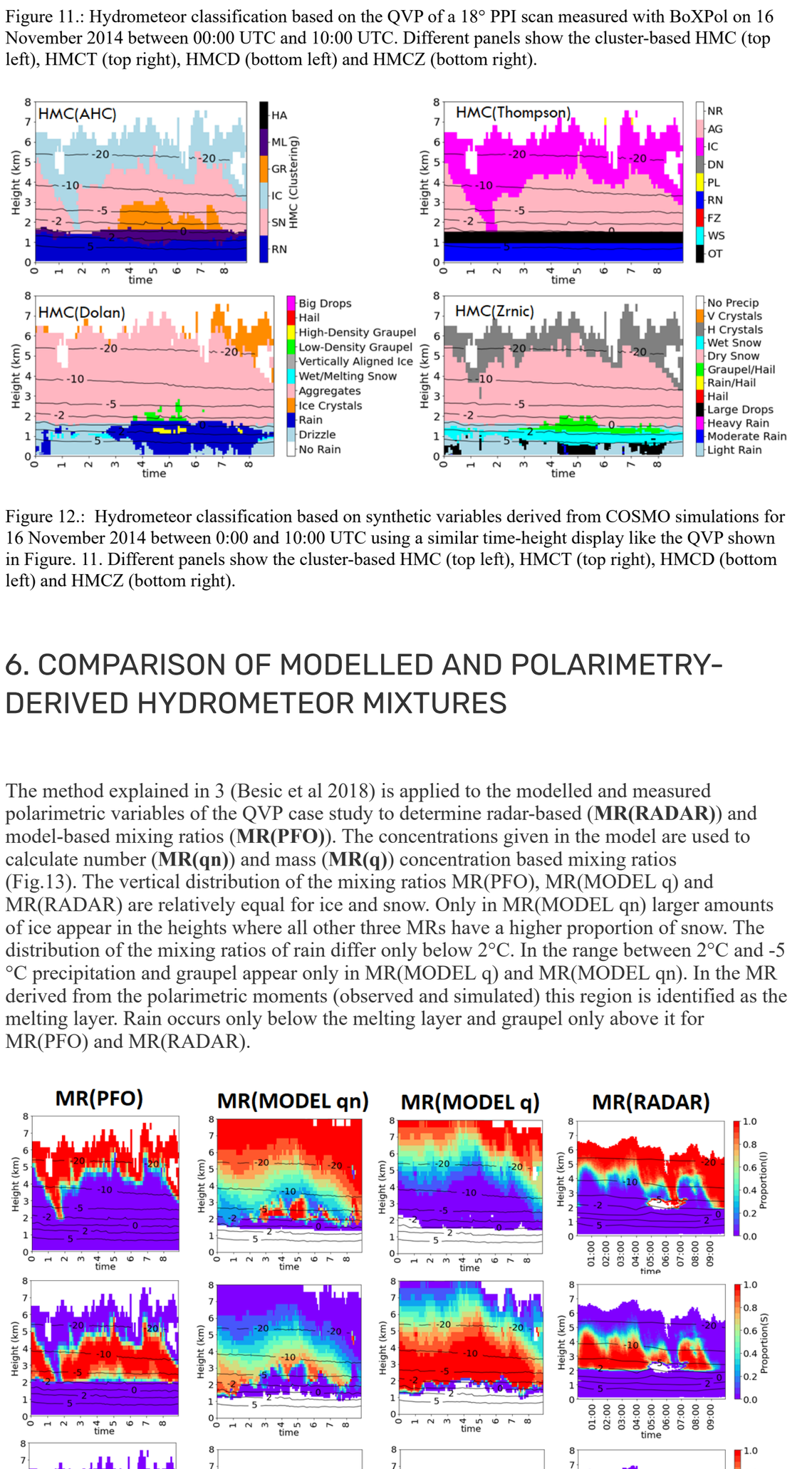

Figure 13.: Hydrometeor mixtures derived following Besic et al. (2018) for the QVP case study (fourth column) and the simulated polarimetric moments (first column) and compared to the mixing ratios derived from the model mass (third column) and number (second column) concentrations. Results are shown for five HM classes: ice (first row), snow (second row), graupel (third row), rain (fourth row) and melting perticles (fifth row). The color indicates the amount of HM proportion.

AUTHOR INFORMATION

Velibor Pejcic

University of Bonn
Institute for Geosciences, Department of Meteorology
Email: velibor@uni-bonn.de

ABSTRACT

A direct comparison of hydrometeor types (HMT) from state-of-the-art hydrometeor classification schemes (HMC) with modelled hydrometeors (ICOL-LAM, operational weather predictions model of the German Weather Service) is challenging, e.g. due to different HMT definitions and numbers and difficulties to identify dominant types in mixtures of hydrometeors. A comparison of published HMCs even revealed significant differences between the membership functions used for the same hydrometeor types (Figure 1), emphasizing again the high uncertainty in scattering simulations for ice hydrometeors because of their complex geometries, dielectric properties, and largely unknown size and orientation distributions. The HMCs were applied to perturbed polarimetric variables observed by the X-band Radar in Bonn (BoXPol) to test their robustness against measurement errors and show that especially in the regions with solid precipitation misclassification in hydrometeor typing occurs often. Thus, a dual strategy to evaluate the hydrometeor type representation in ICON-LAM is presented:

i) Classification after clustering of the data is assumed to reduce the sensitivity of the decision to the uncertainty of scattering simulations. First an agglomerative hierarchical clustering of the radar pixels based on their similarity in multi-dimensional polarimetric signatures is applied, and afterwards for each identified cluster a comparison of the distributions of polarimetric moments with scattering simulations or membership functions for different HMT is performed.

ii) A direct comparison of multivariate simulated and observed distributions of polarimetric moments. These comparisons will be performed for different heights and/or space-time subsets, and for clusters with similar HMT in the model and the observations as identified with the advanced radar-based hydrometeor classification scheme.

Results for a set of case studies observed with the polarimetric X-band radar composite in Bonn, Germany, will be presented.

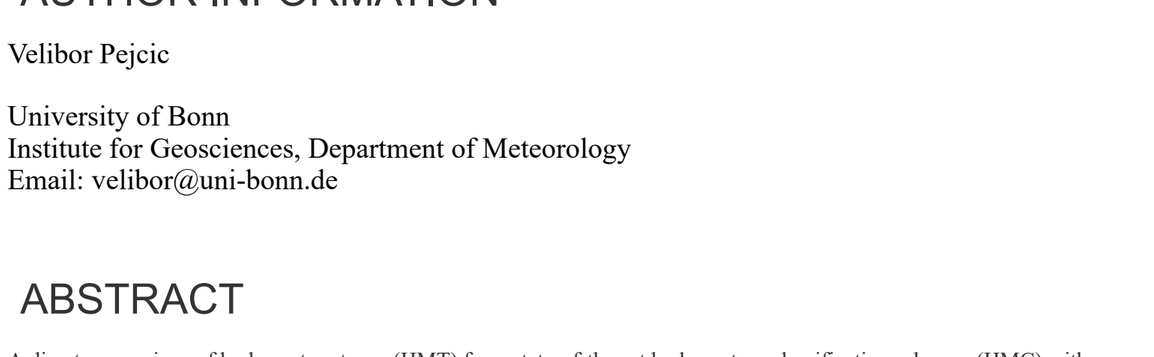

REFERENCES

Grazioli, J., Tuia, D., and Berne, A.: Hydrometeor classification from polarimetric radar measurements: a clustering approach, Atmos. Meas. Tech., 8, 149–170, doi.org/10.5194/amt-8-149-2015, 2015.

Ribaud, J.-F., Machado, L. A. T., and Biscaro, T.: X-band dual-polarization radar-based hydrometeor classification for Brazilian tropical precipitation systems, Atmos. Meas. Tech., 12, 811–837, doi.org/10.5194/amt-12-811-2019, 2019.

Besic, N., Figueras i Ventura, J., Grazioli, J., Gabella, M., Germann, U., and Berne, A.: Hydrometeor classification through statistical clustering of polarimetric radar measurements: a semi-supervised approach, Atmos. Meas. Tech., 9, 4425–4445, doi.org/10.5194/amt-9-4425-2016, 2016.

Zrnić, D.S., A. Ryzhkov, J. Straka, Y. Liu, and J. Vivekanandan, 2001: Testing a Procedure for Automatic Classification of Hydrometeor Types. J. Atmos. Oceanic Technol., 18, 892–913, https://doi.org/10.1175/1520-0426(2001)018<0892:TAPFAC>2.0.CO;2

Straka, J.M., D.S. Zrnić, and A.V. Ryzhkov, 2000: Bulk Hydrometeor Classification and Quantification Using Polarimetric Radar Data: Synthesis of Relations. J. Appl. Meteor., 39, 1341–1372, https://doi.org/10.1175/1520-0450(2000)039<1341:BHCAQU>2.0.CO;2

Evaristo, R. M., X. Xie, S. Trömel and C. Simmer, 2013: A holsitic view of precipitation systems freom macro- and microscopic perspective, 36th Conference on Radar Meteorology, https://ams.confex.com/ams/36Radar/webprogram/Paper229078.html

Dolan, B., and S. A. Rutledge, 2009: A theory-based hydrometeor identification algorithm for X-band polarimetric radars. J. Atmos. Oceanic Technol., 26, 2071–2088.

Besic, N., J. Gehring, C. Praz, Figueras IJ. Ventura,J. Grazioli, M. Gabella, U. Germann, A. Berne, 2018: Unraveling hydrometeor mixtures in polarimetric radarmeasurements – Atmospheric Measurement Techniques11,4847–4866, DOI: 10.5194/amt-11-4847-2018.

Steiner, M., R.A. Houzejer, S.E. Yuter, 1995:Climatological characterization of three-dimensional storm structure from operational radar and rain gauge data Journal of Applied Meteorology 34,1978–2007,DOI:https://doi.org/10.1175/1520-0450(1995)034<1978:CCOTDS>2.0.CO;2.

ACKNOWLEDGMENTS

This scientific contribution by Velibor Pejcic shows some preliminary results from the priority programme SPP-2115 Polarimetric Radar Observations meet Atmospheric Modelling (PROM) (https://www2.meteo.uni-bonn.de/ spp2115) in the project "An efficient volume scan polarimetric radar forward OPERAtor to improve the representaTION of HYDROMETEORS in the COSMO model (Operation Hydrometeors)" funded by the German Research Foundation (DFG, grant TR 1023/16- 1).

The author Velibor Pejcic thanks also Prabhakar Shrestha for providing his COSMO output, Jana Mendrok for extending and providing the polarimetric forward operator and Nikola Besic for his advice on the mixing ration method.